Storm-Scale Ensemble Kalman Filter Assimilation of Total Lightning Flash-Extent Data

EDWARD R. MANSELL

NOAA/National Severe Storms Laboratory, Norman, Oklahoma

(Manuscript received 13 February 2014, in final form 2 July 2014)

ABSTRACT

A set of observing system simulation experiments (OSSEs) demonstrates the potential benefit from ensemble Kalman filter (EnKF) assimilation of total lightning flash mapping data. Synthetic lightning data were generated to mimic the Geostationary Lightning Mapper (GLM) instrument that is planned for the Geostationary Operational Environmental Satellite-R series (GOES-R) platform. The truth simulation was conducted using multimoment bulk microphysics, explicit electrification mechanisms, and a branched lightning parameterization to produce 2-min-averaged synthetic pseudo-GLM observations at 8-km GLM resolution and at a hypothetical 1-km resolution.

The OSSEs use either perfect (two-moment bulk) or imperfect (single-moment, graupel only) microphysics. One OSSE with perfect microphysics included the same electrification physics as the truth simulation to generate lightning flash rates and flash-extent densities (FED). The other OSSEs used linear relationships between flash rate and graupel echo volume as the observation operator. The assimilation of FED at 8-km horizontal resolution can effectively modulate the convection simulated at 1-km horizontal resolution by sharpening the location of reflectivity echoes and the spatial location probability of convective updrafts. Tests with zero flash rates show that the lightning assimilation can help to limit spurious deep convection, as well. Pseudo-GLM observations at 1 km further sharpen the analyses of location (updraft and reflectivity) of the relatively simple storm structure.

1. Introduction

The presence of lightning is an unambiguous indicator of deep electrified convection. Total lightning flash rate [cloud-to-ground (CG) plus intracloud (IC)] has been recognized as being correlated to cycles of deep convection (e.g., Goodman et al. 1988; MacGorman et al. 1989), and in particular to the total graupel contained in a storm cell (Carey and Rutledge 1996; Wiens et al. 2005; Petersen et al. 2005). Numerical simulations of storm electrification have also found a high correlation between total flash rate and graupel echo volume (e.g., Kuhlman et al. 2006; Cohen 2008; Mansell and Ziegler 2013). The CG lightning fraction alone, on the other hand, shows much weaker correlations (MacGorman et al. 1989; Wiens et al. 2005). Therefore, total lightning is a much more attractive observation from a data assimilation perspective for forecast models at sufficient resolution to explicitly predict convective elements without a convection parameterization scheme (i.e., convection-allowing resolution with horizontal grid spacing $\lesssim$4 km).

Total lightning detection is currently available over land for local or extended regions from various time-of-arrival systems such as Lightning Mapping Arrays (LMAs; Rison et al. 1999), the Lightning Detection Network in Europe (LINET) system (Betz et al. 2009), the Earth Networks Total Lightning Network (e.g., used by Fierro et al. 2012), and the upgraded U.S. National Lightning Detection Network (Nag et al. 2014). The detection efficiency of ground-based total lightning systems drops off rapidly outside the network, however, so they are unable to cover large oceanic regions. Long-range systems, such as the Met Office ATDnet system and the World Wide Lightning Location Network (WWLLN; Lay et al. 2004), only detect the most strongly radiating lightning discharges, which are primarily CG return strokes.

The upcoming Geostationary Operational Environmental Satellite-R series (GOES-R; Gurka et al. 2006; Goodman et al. 2012) is planned to carry the Geostationary

Corresponding author address: Edward R. Mansell, NOAA/National Severe Storms Laboratory, 120 David L. Boren Blvd., Norman, OK 73072.
E-mail: ted.mansell@noaa.gov

DOI: 10.1175/MWR-D-14-00061.1

Lightning Mapper (GLM) instrument (Goodman et al. 2013), which will detect total lightning optically in a manner similar to the Lightning Imaging Sensor (LIS; Christian et al. 1992; Mach et al. 2007). The GLM promises fairly high resolution (8–12 km) and high detection efficiency of total lightning (>70% for day and night) over both continents and oceans. This makes it a rich potential data source for convection-permitting model forecasts that extend over oceans or any area without weather radar coverage (e.g., tropical mesoscale convective systems and cyclones).

Lightning has been assimilated into mesoscale models (≥10-km grid spacing) via various single forecast nudging techniques, for example by modifying the latent heating rates from the convection parameterization scheme (CPS; e.g., Alexander et al. 1999; Chang et al. 2001; Pessi and Businger 2009), forcing the CPS directly (Mansell et al. 2007), or by adjusting the humidity profile and thereby encouraging the CPS to activate (Papadopoulos et al. 2005). These studies all utilized CG lightning data, and Mansell et al. (2007) also showed an additional benefit of including total lightning data. Hakim et al. (2008) first used the ensemble Kalman filter (EnKF) method (Evensen 1994; Houtekamer and Mitchell 1998; Whitaker and Hamill 2002) to assimilate long-range lightning data (primarily CG), which were first converted to convective rainfall rates. At convection-allowing scales, on the other hand, little work has utilized lightning data. Fierro and Reisner (2011) and Fierro et al. (2012) forced simulated convection at observed lightning locations by adding water vapor to maintain a minimum humidity within a confined layer in the column, which adds buoyancy and promotes updrafts and cloud formation. Fierro et al. (2012) used total lightning stroke data (with >50% IC detection efficiency), and the humidity forcing was proportional to the lightning flash rate. Their nudging method was effective for initiating convection where lightning was detected, but did not attempt to suppress spurious convection or otherwise modulate the convection.

Ground-based lightning detection networks that cover large areas typically provide only time, latitude, and longitude of lightning impulses with the highest-power radiation, but give no information on the spatial extent of discharges. Mapping systems can provide detailed horizontal and vertical extents (e.g., LMA) or varying resolutions of horizontal extent (e.g., LIS, GLM, and 2D interferometers). Mapping allows for the construction of flash-extent density (FED), which counts the rate of lightning flashes extending over each cell or pixel in a horizontal 2D grid. Thomas et al. (2000) found a good comparison in horizontal area coverage between LMA and LIS, particularly for flashes within the upper half of the storm. The lower resolutions of LIS and GLM (4 and 8 km) compared to LMA (tens of meters) leads to coarsening and a high bias in coverage, at least in terms of minimum area.

The current work demonstrates assimilation of pseudo-GLM total lightning FED data using the EnKF method in an observing system simulation experiment (OSSE) at convection-resolving scale. (In this paper, "flash rate" generally refers to the storm cell as a whole, whereas FED refers to a pixel-level flash rate.) OSSEs are frequently used to estimate the impact of data from instruments that are not yet operational. Here, simulated pseudo-GLM lightning flash rates are generated from a thunderstorm simulation that includes physical parameterizations of electrification and lightning (Mansell et al. 2002). The synthetic observations are then assimilated into ensembles with perfect or imperfect physics and with or without electrification.

2. OSSE setup

The OSSE begins with a "truth" or "nature" simulation of an electrified convective storm. This study used the Collaborative Model for Multiscale Atmospheric Simulation (COMMAS) within an EnKF framework (Dowell and Wicker 2009). The truth simulation employed a full two-moment bulk microphysics parameterization that predicts mass mixing ratio and particle number concentration for six hydrometeor classes (cloud droplets, rain, cloud ice, snow, graupel, and hail) as well as the average bulk particle densities of graupel and hail (Mansell et al. 2010). Electrification parameterizations followed Mansell et al. (2005), including noninductive charge transfer between graupel particles and ice–snow particles, inductive charging between graupel and small droplets, and small ion processes (e.g., generation by cosmic rays, recombination, attachment to hydrometeors, drift, and corona point discharge at the ground). For this study, noninductive graupel-ice charging was based on the laboratory results of Saunders and Peck (1998) combined with Brooks et al. (1997) as in Mansell et al. (2010).

The environment was specified using the analytical sounding of Weisman and Klemp (1982) with a surface temperature of 300 K and a boundary layer vapor mixing ratio of 14 g kg^{-1}, yielding a convective available potential energy (CAPE) of 2050 J kg^{-1} and convective inhibition (CIN) of 21.6 J kg^{-1} for a mixed-layer parcel. The u component of wind increases linearly from 0 m s^{-1} at the surface to 10 m s^{-1} over the lowest 5000 m. For the truth simulation, random thermal perturbations (~0.1 K) were introduced into the boundary layer, and convection was initiated through a vertical acceleration term in a spheroidal region (center value of 0.03 m s^{-2})

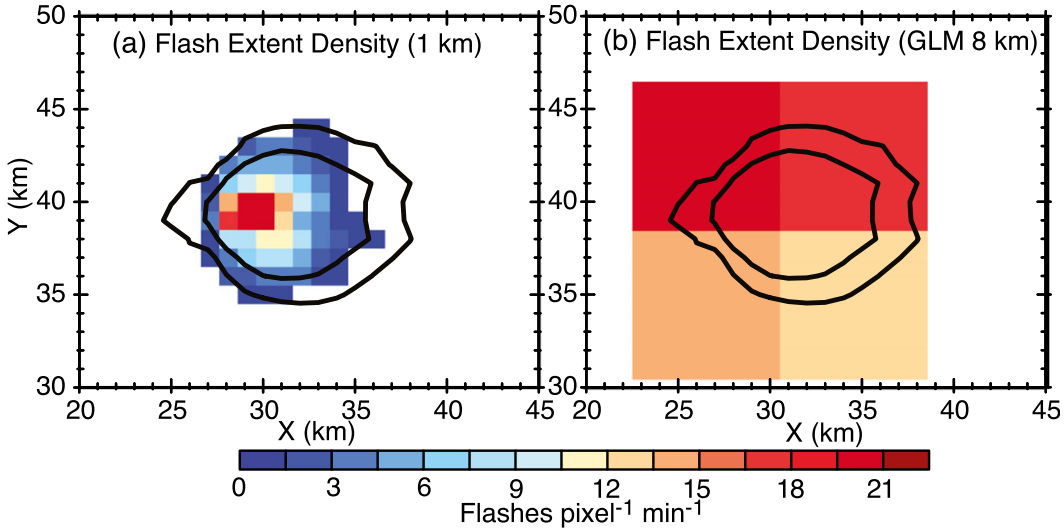

FIG. 1. Example of 2-min flash-extent densities (38–40 min) from the truth simulation at (a) 1-km and at (b) 8-km grid spacing. Contours show composite reflectivity at 30 and 45 dBZ.

for 20 min (Mansell et al. 2010). The truth simulation was run for 90 min, by which time the storm had substantially decayed. Convection in the ensembles was initiated with four warm bubbles (maximum positive temperature perturbation of 1 K) whose centers were randomly placed within a 12 km × 12 km region around the initial area of forcing for the truth simulation, often resulting in two separate storm cells in any given member. The computational grid for all simulations used an 80 km × 80 km × 18 km domain with 1-km horizontal grid spacing and 40 vertical levels with variable spacing (200 m for the lowest level, stretching up to 700 m aloft).

The synthetic GLM observations were calculated by processing the lightning channel paths from the truth simulation to the 8- and 1-km grids at a 2-min time resolution. Detection efficiency of 100% was assumed, which certainly is an overestimate and ignores any diurnal effects on optical detection. The ensemble with electrification stored 8-km native FED, which were incremented for each simulated lightning flash. A comparison of 1- and 8-km FED from the truth simulation is shown in Fig. 1. The FED counts the number of flashes that extend over a given horizontal area, thus the 8-km FED could have higher counts than the maximum 1-km FED value within the same area because multiple flashes could enter an 8-km pixel without overlapping each other on the 1-km grid. The 8-km resolution approximately corresponds to the expected resolution at nadir of the planned GLM instrument on the GOES-R series satellites.

Initial tests found that brief excursions in flash rate caused unreasonable changes in the storm (e.g., graupel mass), so the synthetic FED data were smoothed in time with a centered 6-min simple averaging. For example, Fig. 2b shows 1-min storm flash rates, 6-min smoothed flash rates, and the graupel volume. The graupel volume changes smoothly in time, corresponding better to the smoothed flash rates. The smoothed truth FEDs were assimilated every 2 min for the entire 90-min simulations. At 8 km, this amounts to 100 observations per assimilation (6400 observations for 1-km pixels). The truth storm moved across the domain during the course of the simulation, which allowed it to cross multiple 8-km pseudo-GLM pixels. The pseudo-GLM observations had no added bias or random error, and the assimilation assumes an observation uncertainty of 2 flashes per pixel per minute.

Data assimilation used the ensemble square root filter (EnSRF) of Whitaker and Hamill (2002) as implemented in Dowell and Wicker (2009). Because observation operator values may be generated by the model physics, the Anderson and Collins (2007) parallel algorithm was employed (see the appendix for details). The usual serial EnSRF algorithm requires the observation operator to be calculated from the model state as each new observation is assimilated. This can be a problem when an observation operator is an integrated quantity, such as surface rain accumulation, or, in this case, a flash rate that is produced by the model physics. The parallel algorithm treats the values returned by observation operators in a similar manner as state variables, and these "operator variables" are then directly adjusted by the filter in a similar manner to the state variable updates. In the other cases where a flash rate is estimated

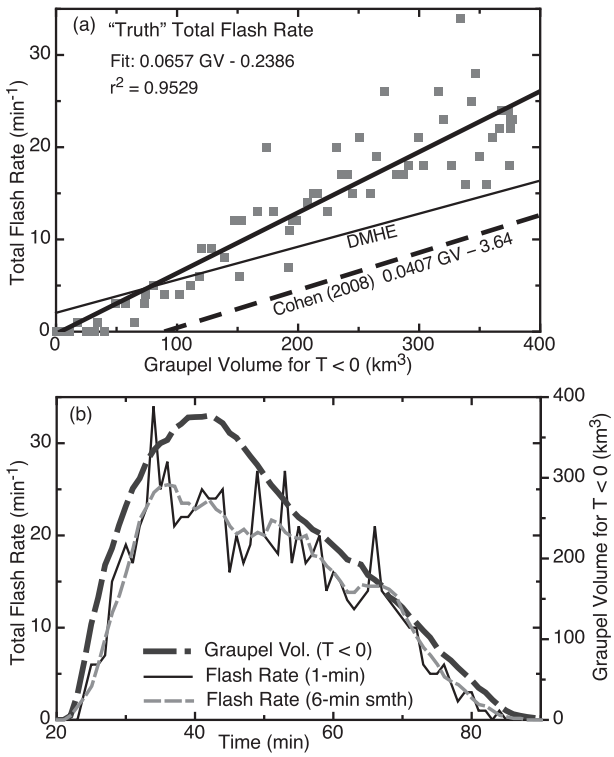

FIG. 2. (a) Flash rate relationship with graupel echo volume for the truth simulation and from Cohen (2008) for isolated storms. The peak flash rate was 34 min^{-1}. The DMHE line shows the linear correlation derived from the results of that experiment. (b) Time series from the truth simulation for graupel volume and raw and smoothed storm flash rates.

from the model state, the parallel algorithm was not required but was still used to maintain consistency.

All experiments, with or without data assimilation, used ensembles having 36 members. Qualitatively similar results were also obtained using 20 members or 72 members. All members used the same environment as the truth simulation, and the initial thermal perturbations provided sufficient variability in the members such that methods like covariance inflation or additive noise were not needed. The Kalman gain was modulated by a horizontal localization factor that monotonically rolls off from 1 to 0 at a radius $R = 15$ km using the function of Gaspari and Cohn (1999). (The localization radius was 4 km for the 1-km FED experiment.) Note that the localization factor drops to 0.5 at about $R/3$ and to 0.2 at $R/2$, so the effective localization radius is roughly 7.5 km. The vertical localization radius is effectively set to infinity, as the pseudo-GLM data have no direct height information. The filter updated all state variables (e.g., temperature, winds, hydrometeor quantities) except pressure, subgrid turbulent energy, and electric charge.

Perfect microphysics model experiments used the same double-moment scheme with hail (DMH) as the truth simulation (Table 1). Imperfect experiments used the single-moment (SM) version of the same microphysics scheme but without the hail category. Single-moment intercept parameters for rain and graupel were set to $n_{\mathrm{or}} = 8 \times 10^5\,\mathrm{m}^{-4}$ and $n_{\mathrm{og}} = 4 \times 10^5\,\mathrm{m}^{-4}$, and graupel bulk density was predicted for both DMH and SM. Although the hail category was included in the truth simulation, not much hail was produced, and total hail mass was generally at least an order of magnitude smaller than total graupel mass.

The DMHE experiment employed electrification physics in all members (as in the truth simulation) to generate flash rates, and all other experiments used one of two linear relationships between flash rate and graupel echo volume (volume of the storm with graupel mixing ratio $> 0.5\,\mathrm{g\,kg}^{-1}$) as the observation operator. The first relationship was the linear fit from the truth simulation (Fig. 2a). The second relationship came from Cohen (2008) (also shown in Fig. 2a), who fitted multiple strong, isolated storms that were simulated with an earlier version of the two-moment microphysics. The Cohen fit was included to assess differences arising from bias errors in the observation operator relationship, as this fit underestimated the true flash rate by about

TABLE 1. Options for truth simulations and ensemble experiments. The "perfect" microphysics scheme was the double-moment bulk scheme with hail (DMH), and the "imperfect" was the single moment (SM) with hail deactivated.

Expt	Microphysics scheme	Electrification physics	Flash rate method	Lightning assimilation
Truth	DMH	Yes	—	—
DMHE	DMH	Yes	Native 8-km FED	Yes
DMH-NoDA	DMH	No	—	No
DMHC	DMH	No	Cohen fit	Yes
DMHT	DMH	No	Truth fit	Yes
DMHT-1kmob	DMH	No	Truth	Yes
SMC	SM	No	Cohen fit	Yes
SMT	SM	No	Truth fit	Yes
SM-NoDA	SM	No	—	No
SMZ (all zero FED)	SM	No	Truth fit	Yes

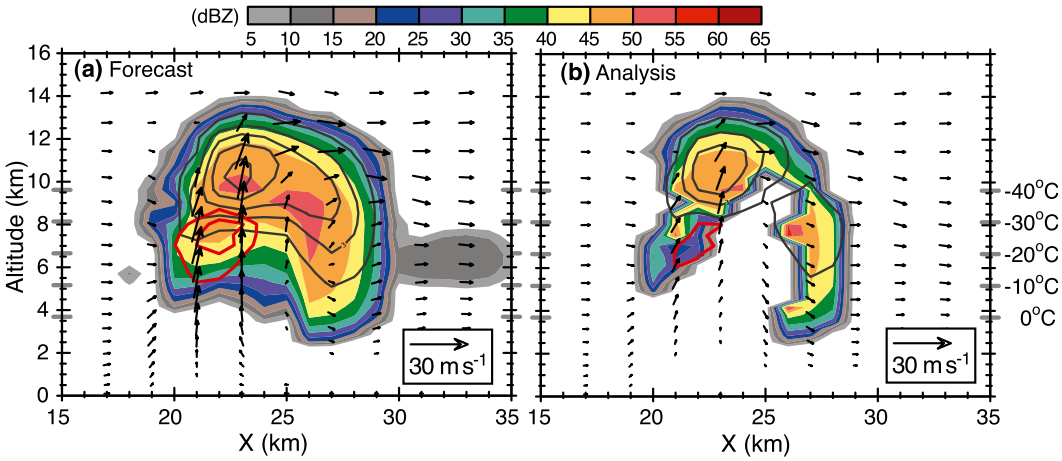

FIG. 3. (a) Forecast and (b) analysis of member 15 of experiment DMHT for the assimilation at 20 min showing the reduction of excessive convection. Graupel mass mixing ratio (black contours at 1, 3, 5, 7, and 9 g kg^{-1}) and rain mixing ratio (red at 0.5 and 1.0 g kg^{-1}) are overlaid on simulated radar reflectivity and wind vectors.

a factor of 2. The GLM observation operator was calculated by summing the graupel echo volume in a 12-km-wide square area centered on the pseudo-GLM pixel location and then applying the linear relationship. Larger and smaller areas were tested, and 12-km width seemed to be the optimal size for 8-km GLM pixels to include the influence of lightning originating just beyond the edges of a pixel. A 4-km width was used for the 1-km observations experiment along with a localization radius of 4 km.

3. Results and discussion

a. Overall results

A key advantage of the EnKF technique over nudging is the covariances used to update unobserved state variables. The thermal bubble initialization of the ensemble members resulted in faster development of convection than in the truth simulation, so some suppression was needed particularly at the early stage. An example EnKF analysis update to a member in the premature storm phase at a time when there was not any lightning in the truth simulation is shown in Fig. 3. Updraft speeds and graupel and rain contents are noticeably reduced by the single update.

The premature growth phase caused the initial spike in FED root-mean-squared errors (RMSE; Fig. 4a). The ensembles also developed sufficient initial spread (Fig. 4b) to weight the Kalman gain toward the observations and reduce the initial errors. All of the lightning assimilation experiments had FED RMS errors well below the no-assimilation control ensembles (DMH-NoDA and SM-NoDA). At 20 min, the experiments using the truth graupel–lightning relationship showed higher RMSE than the corresponding Cohen fits, but this is a result of a biased operator. For a given overshoot in graupel volume, the Cohen fit yields a lower flash rate than the truth fit (Fig. 2a) and thus a smaller difference from a zero flash rate. The errors at later times were comparable for the DMH and SM experiments without electrification. The 1-km observations test (DMHT-1kmob) was better at isolating the convection than the 8-km resolution observations and had mostly lower FED RMSE but also correspondingly lower spread.

The perfect model experiment DMHE had larger FED RMSE values than the non-electrified assimilation experiments, but also maintained much higher spread (Fig. 4b). The higher error and spread resulted from greater variability in the predicted FED than the parameterized rate based on graupel volume (Fig. 2b), particularly since the comparison truth is the time-averaged FED. This flash rate variability arises from dependence on more variables than the graupel echo volume as well as the history of charge separation and the random nature of the discharges themselves. The non-electrified experiments gradually lost spread because of the linear relationship used between graupel echo volume and flash rate and the generally slow variation in graupel echo volume (Fig. 2b), but they reached a minimum value of about 1.5 by 40 min. This minimum spread is likely maintained by the variability in storm cells that arise from the randomly located initial thermal perturbations. The lightning assimilation operates at a sufficiently large scale that smaller-scale perturbations are maintained and can grow during assimilation cycles. The drop in spread and error after about 80 min results from the dissipation (or suppression) of convection in the mean.

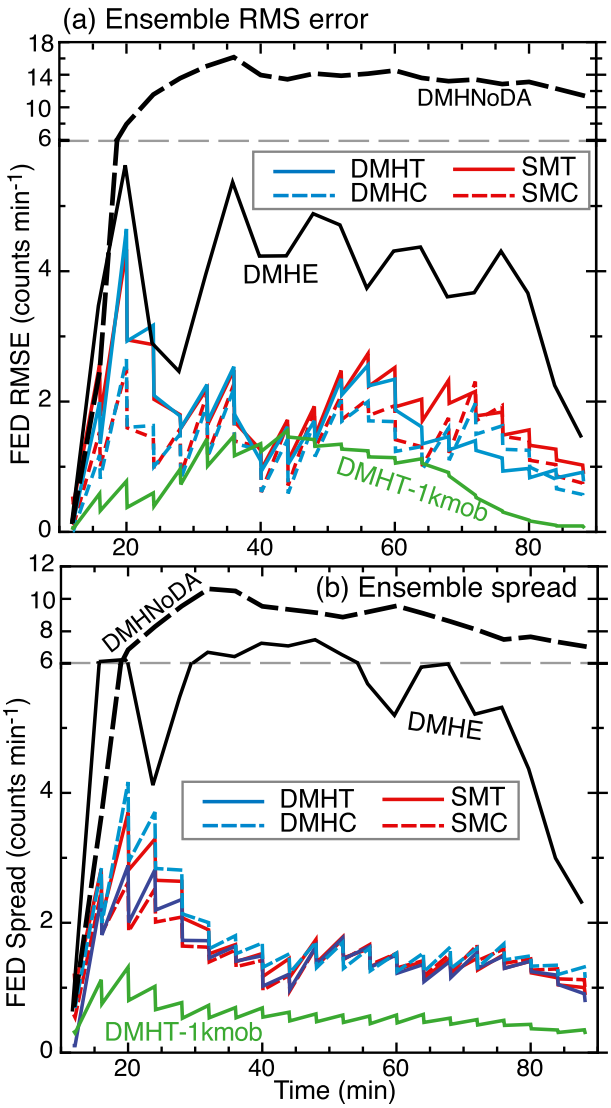

FIG. 4. Ensemble prior (a) RMS error and (b) spread in lightning flash rates. (Posteriors cannot be calculated for DMHE–DMHE2.) Forecast statistics for DMH-NoDA are shown for comparison, using a scale change indicated by the horizontal dashed line. Statistics are for 4-min bins, such that each bin time includes two assimilation cycles.

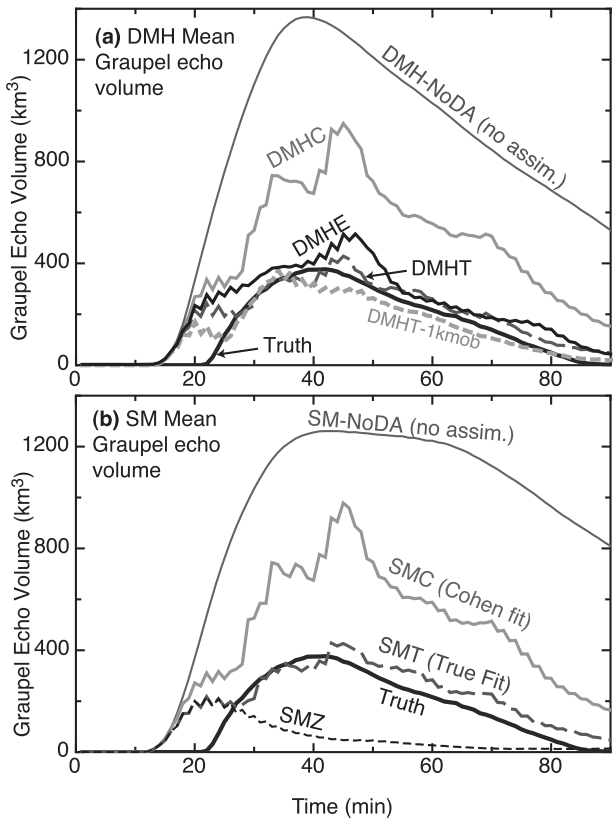

FIG. 5. Time series (1 min) of averaged graupel echo volume for (a) perfect model experiments (DMH) and (b) imperfect model experiments (SM). The 1-min oscillations are a result of values being intermediate between analyses and forecasts (i.e., either 1- or 2-min forecasts from the analyses).

b. *Graupel volume, hydrometeor mass, and updraft mass flux*

Graupel volume and updraft mass flux were examined in addition to the RMSE of flash-extent density, because the observation-space diagnostics only express how well the ensembles match the synthetic observations. All of the assimilation experiments succeeded in adjusting the mean total graupel volume toward the truth simulation (Fig. 5). The experiments that used the true graupel–lightning relationship (DMHT and SMT) did similarly well despite the imperfect microphysics in SMT. Given the high correlation between graupel volume and flash rate, the impact of 1-km observations (DMHT-1kmob) on graupel volume was relatively small compared to the 8-km observations. Full suppression (zero flash rates) in SMZ (Fig. 5b) did fairly well in reducing the graupel volume down to minimal values but took some time to do so, suggesting a reasonable ability to reduce spurious convection.

The explicit lightning case DMHE was nearly as good as the truth diagnostic observation operator (DMHT and SMT) for graupel echo volume (Fig. 5a). The Cohen (2008) operator (DMHC and SMC) exhibited an expected high bias in graupel volume because the operator flash rate is lower for a given graupel volume compared to the truth fit (Fig. 2a). A linear regression line for the DMHE ensemble is shown in Fig. 2a for comparison with the true and Cohen (2008) relationships. The DMHE line has a flatter slope than the true relation and has a slightly positive intercept that would predict lightning with zero graupel volume, but less of a bias than the Cohen operator at lower graupel volumes.

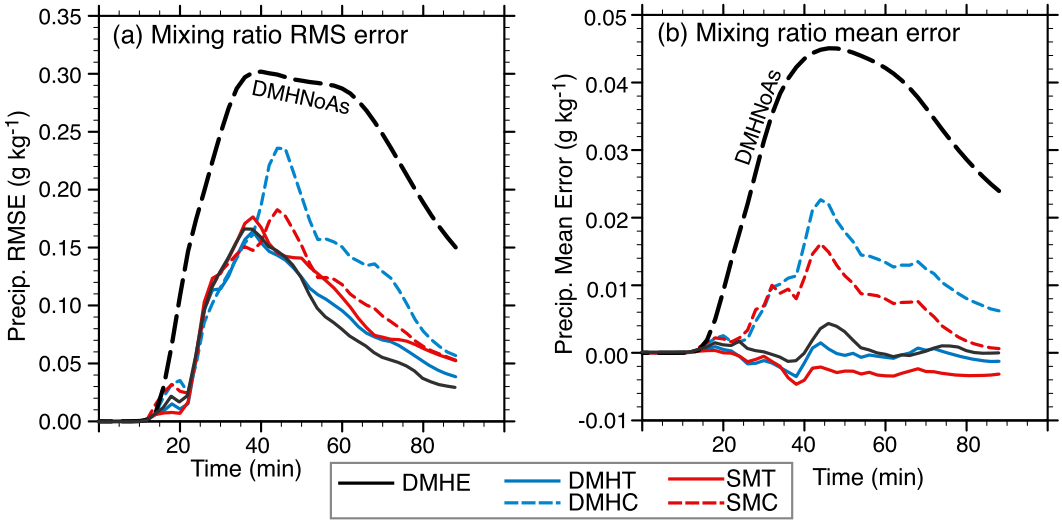

FIG. 6. Domain-averaged (a) RMS errors and (b) mean errors in total precipitation mixing ratio (sum of graupel, hail, rain, and snow) between the truth simulation and the analysis means.

The RMS and mean errors in the precipitation hydrometeor mass (sum of rain, graupel, hail, and snow mixing ratios; Fig. 6) provide a more quantitative evaluation of the assimilation. DMHE has the best overall performance in terms of RMSE, but on average has similar bias error magnitudes as DHMT. A high bias is again seen with the Cohen operators (DHHC and SMC) along with higher RMS error, particularly after 40 min. The mean errors from the single-moment experiments (SMT and SMC) show a negative offset from the corresponding double-moment schemes, suggesting a bias toward lower mass in the choice of distribution parameters (intercepts for rain and graupel).

Updraft mass flux is an integral quantity that is one of many possible measures of convection intensity, and it is less directly correlated to lightning flash rate than graupel volume in storm simulations (Cohen 2008). Thus, it serves as a good test of the model covariances. The mass fluxes in Fig. 7 were taken at the −20°C level, which is in the heart of the mixed-phase region where electrification is most active. All of the assimilation experiments achieved an initial correction in mass flux around 15–30 min, but DMHC and SMC had the least improvement after 30 min. Similar to the graupel volume, the DMHE result was close to DMHT but between DMHT and DMHC. Here the nonelectrical perfect model DMHT performed slightly better in general than the imperfect SMT, particularly around 50 min where SMT allowed the mass flux to grow. The 1-km observation case (DMHT-1km) did well other than a large error peak at 30–40 min from a spurious secondary updraft. The suppression test SMZ succeeded in reducing the mean updraft mass flux well below the truth value after 30 min.

c. *Radar reflectivity and updraft location*

The various pseudo-GLM lightning assimilation experiments had definite effects on the ensemble mean reflectivity structure (Fig. 8, at 40 min), and acted to

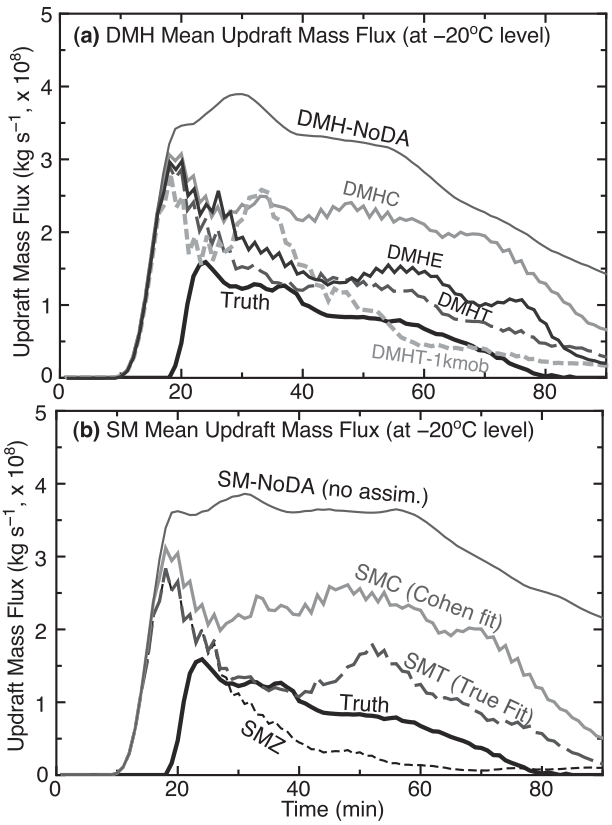

FIG. 7. As in Fig. 5, but updraft mass flux.

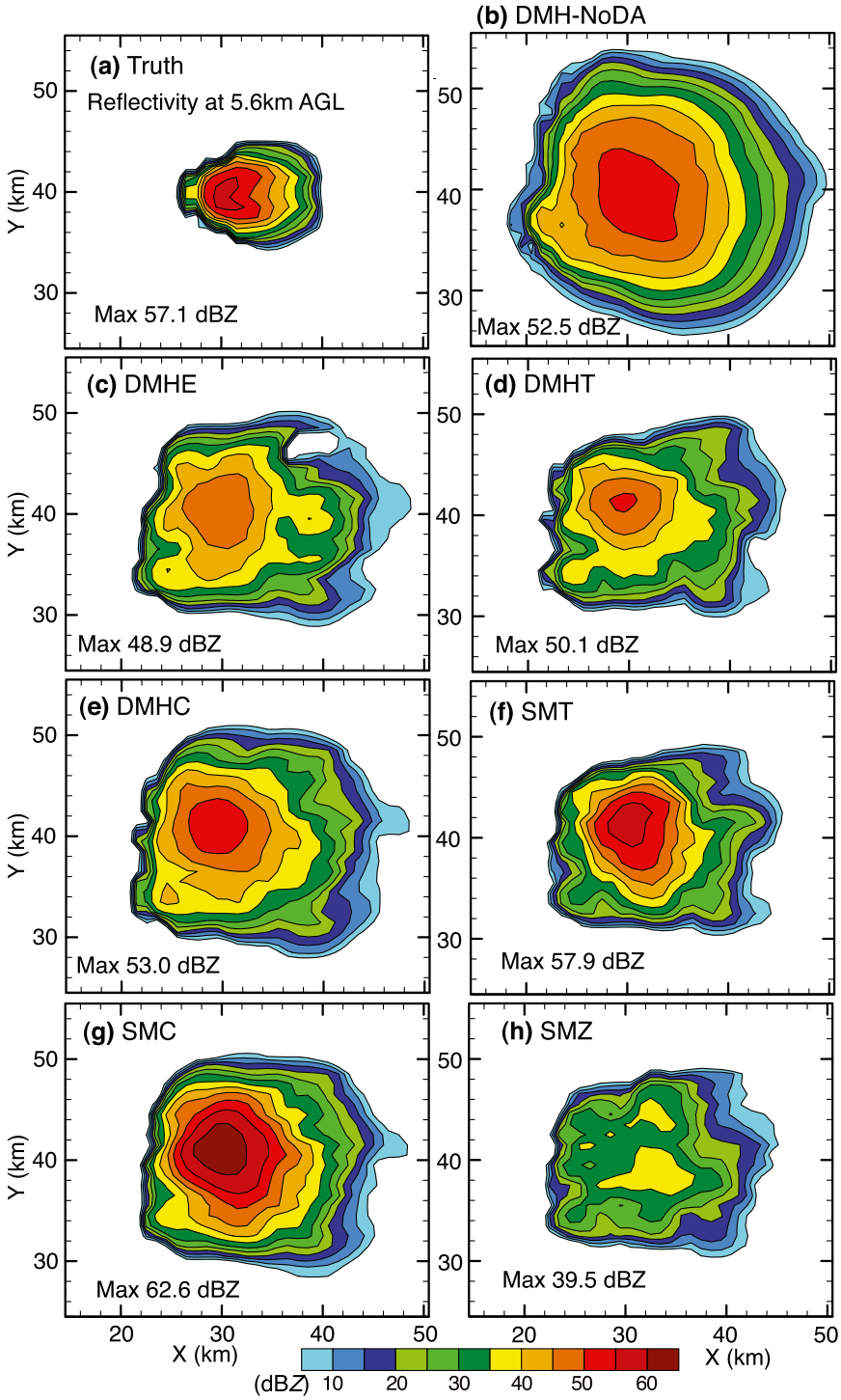

FIG. 8. Simulated radar reflectivity at 5.7 km AGL after 40 min of simulation for (a) truth simulation and (b)–(h) ensemble means. SM-NoDA was very similar to (b) and is not shown.

restrict the reflectivity area compared to the unconstrained pure forecast ensemble (Fig. 8b). The perfect model DMHT experiment (Fig. 8d) yielded mean reflectivity areas (40–50 dBZ) closest to the truth simulation (Fig. 8a). By comparison, SMT allowed too large an area of higher reflectivity. The DMHE (Fig. 8) again fell somewhere between DMHT and DMHC in terms of reflectivity area, which is consistent with their

relative graupel echo volumes and updraft mass fluxes. (Note that the ensemble radar reflectivity was calculated from the mean state variables and not the average of the individual logarithmic reflectivity values.)

Overall, the assimilation experiments (Figs. 8c–g) allowed a greater circumscribed area of reflectivity (>20 dBZ) than the truth simulation. This broadening is not entirely a consequence of the coarse 8-km resolution of the pseudo-GLM observations, although this can cause a small cell to appear to be as large as 16 km by 16 km, depending on how many pseudo-GLM pixels its lightning footprint overlaps. Incomplete suppression of spurious cells, as in the SMZ result, also contributes to the broadened reflectivity. The resolution of the coverage may be less important, however, for larger storms or larger organized systems, such as squall lines and tropical cyclones. Also notable is a slight northward bias caused by the southward offset of the synthetic observation pixels relative to the true storm, which resulted in slightly higher synthetic 8-km FED rates on the north side of the storm (Fig. 1b). DMHE had slightly less position bias, which along with the low bias in reflectivity suggests that it was less successful at producing a cell in a common location across the ensemble members.

The case with zero assumed flash rate (SMZ, Fig. 8h), did a fairly good job of limiting the analysis mean reflectivity where little to no lightning might be expected. A majority of the SMZ members, however, still had cells with reflectivity values exceeding 50 dBZ at 40 min (not shown). The other cases such as DMHT also occasionally had one or more spurious cells. DMHT-1kmob, on the other hand, suppressed spurious cells better than DHMT with 8-km observations. The DMHT-1kmob experiment had a similarly wide area of lower reflectivity values (Fig. 9a) that resulted from a similar incomplete suppression of convection as seen in the SMZ experiment (Fig. 8h). The enhanced suppression in DMHT-1kmob appears to result from better definition of the main cell, perhaps providing more accurate subsidence and cold outflow.

A test with 1-km observation in the SMZ case still allowed random cells to persist, suggesting that the density of observations alone is not sufficient to suppress all deep convection. Rather, the persistence of cells within the SMZ members may be more an issue with the EnKF requirement for a Gaussian distribution. Specifically, when only one or two members have storm cells in a given location and most other members have none, the distribution of related state variables (updraft, hydrometeor mixing ratios, etc.) is most likely bimodal and might be improved with a very large ensemble size. A test with 72 members, however, showed little improvement, which underscores the difficulty of controlling spurious storms when the environment has substantial instability but minimal inhibition.

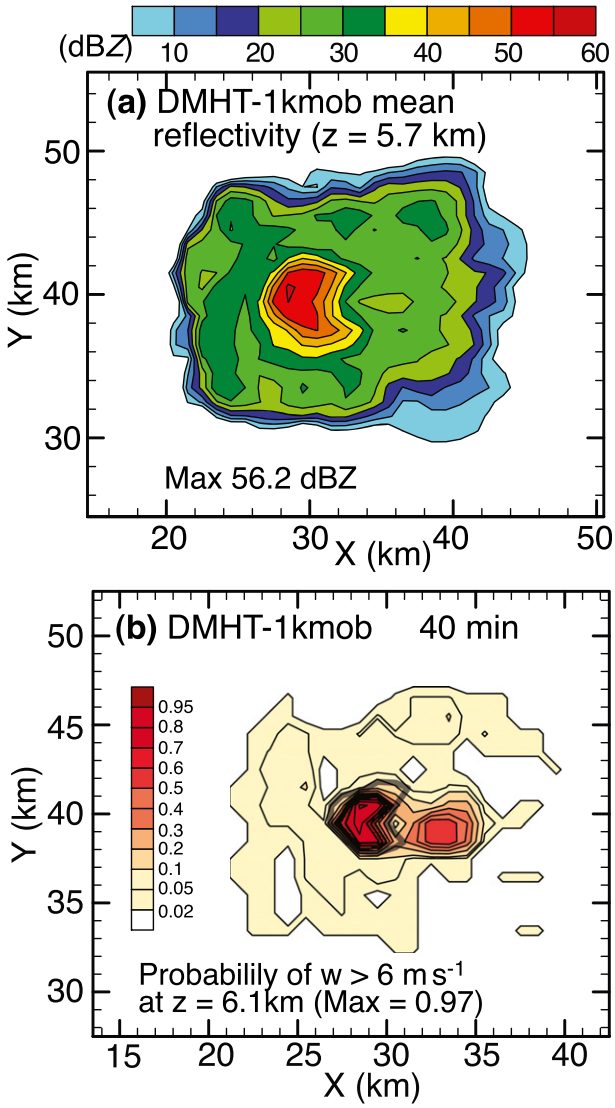

FIG. 9. (a) Ensemble analysis mean simulated radar reflectivity and (b) ensemble analysis probability of updraft >6 m s^{-1} at 40 min for the 1-km observations experiment. The thick black curve in (b) denotes the 6 m s^{-1} contour of the truth simulation.

The probabilities of updraft greater than 6 m s^{-1} (Fig. 10) illustrate the ability of the assimilation to isolate the main updraft compared to the unconstrained ensemble at 40 min. Similar to the mean reflectivity, updrafts were reasonably suppressed outside the main cell. The northward bias is again evident for DMHT (Fig. 10b). DMHE showed no obvious north–south bias, but had lower probabilities that again indicate less success at producing a common cell. DMHT-1kmob did very well at focusing high probabilities within the area of the actual updraft (Fig. 9b), but also allowed a spurious

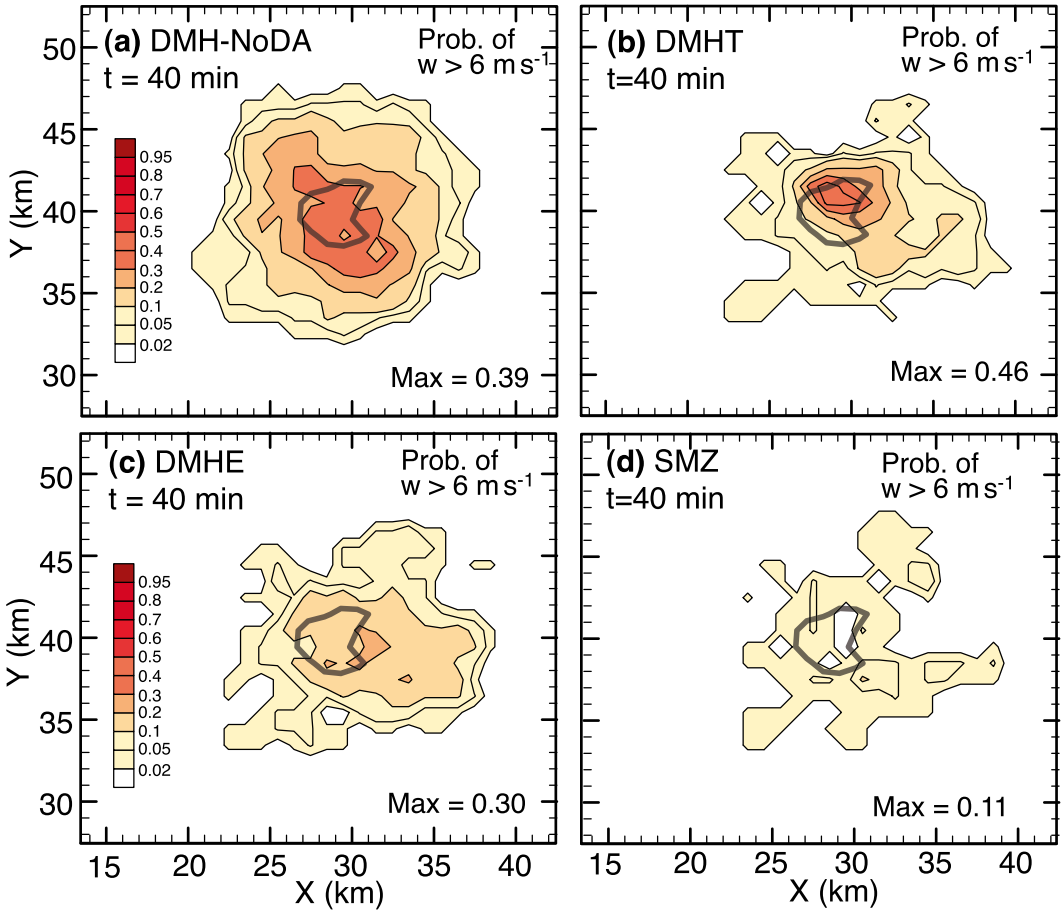

FIG. 10. Ensemble probabilities of updraft >6 m s^{-1} at 6.1-km altitude for (a) DMH-NoDA, (b) DMHT, (c) DMHE, and (d) SMZ. The thick black curves denote the 6 m s^{-1} contour of the truth simulation.

secondary area of updraft to the east. The secondary updrafts contributed to the excessive updraft mass flux at 30–40 min seen in DMHT-1kmob (Fig. 7a).

4. Conclusions

This OSSE study has demonstrated the feasibility of total lightning FED data assimilation in an EnKF framework at convection-resolving scales for modulating the intensity of simulated convection (e.g., in terms of echo volume or updraft mass flux) and helping to suppress spurious deep convection. Better isolation of the storm was still achieved with biased lightning operators and imperfect physics. Convection suppression is reasonably effective in the mean, although the moderate instability and low convection inhibition allow random nonoverlapping cells to persist in individual members regardless of the data density. Synthetic GLM observations of flash-extent density were used at the expected nadir pixel size of 8 km and tested at a hypothetical 1-km size such as could be derived from existing land-based lightning mapping networks.

A perfect model ensemble normally has the best performance in an OSSE framework (e.g., Meng and Zhang 2007). In this case, however, the perfect model (DMHE) performed slightly worse overall than a well-tuned linear lightning observation operator (DMHT). Typical observations, such as used by Meng and Zhang (2007), are directly related to instantaneous state variables (e.g., surface temperature, winds, and radar reflectivity). Lightning flash rate, however, is a time-integrated result of particle interactions and motions, resulting in a much more complex and nonlocal relationship to the state variables. As seen in Fig. 2b, the flash rate is noisy, and the DMHE experiment used 2-min flash rates from the ensemble (without 6-min averaging), which likely hampered to its ability to isolate a cell in the ensemble. The DMHT ensemble with perfect physics and the true graupel–flash rate relationship performed quite well in reproducing the mean graupel echo volume, and updraft mass flux, and

was generally better than the SMT ensemble with simpler microphysics.

Results for DMHE might be improved by running the members past the analysis time to be able to generate a smoother averaged flash rate, but at a cost of greater computation. Another clue to the DMHE performance is the flash rate to graupel volume fit line in Fig. 2a (labeled DMHE) generated from the entire ensemble for all 1-min intervals with nonzero graupel volume. The DMHE fit has a slope similar to the Cohen line, suggesting that the overly strong initial convection may have skewed the lightning relationships compared to the truth simulation.

Lightning data can pinpoint mixed-phase deep convection that can be hard to identify in otherwise data-sparse regions (e.g., oceans), where its use in data assimilation is expected to have the greatest impact. Lightning data are not expected to compete with radar data, which have much higher density and information content. Lightning data may still add value to radar at small additional expense, though this has not been tested here. Any diagnostic lightning FED operator will likely need to be tuned for real data cases, and although Petersen et al. (2005) showed large scatter in flash rates, their results suggest that the overall systematic bias could be minimized.

Acknowledgments. This work was supported by the NESDIS program, which is under the auspices of the National Oceanic and Atmospheric Administration (NOAA) of the U.S. Department of Commerce, through Grant NA08OAR4320904 with the Cooperative Institute for Mesoscale Meteorological Studies. Computer resources were made available on the NOAA–NASA-funded JCSDA supercomputer operated by NASA's Goddard Space Flight Center. Thanks are extended to David Dowell and Louis Wicker for development of the EnKF system and to Donald MacGorman and Conrad Ziegler. Comments from Greg Hakim, Fuqing Zhang, Alex Fierro, and two anonymous reviewers resulted in further improvements.

APPENDIX

Kalman Filter Equations

A brief description is given here concerning the implementation of the Anderson and Collins (2007) parallel EAKF (ensemble adjustment filter) algorithm for the Whitaker and Hamill (2002) square root filter. The notation from Dowell et al. (2004) and Dowell and Wicker (2009) is adapted for consistency. The first step is to produce the initial observation operators $H(\mathbf{x}_n^f)_o^{k=0}$ for each observation $o = 1, K$ for all ensemble members $n = 1, N$, as well as the mean values $\overline{H(\mathbf{x}^f)}_o^{k=0}$ for each observation, where the superscript $k = 0$ indicates the initial value before any observations have been assimilated ($k = 0, K - 1$). The observation operator can be a direct function of the instantaneous state vectors $\mathbf{x}$ (e.g., wind speed or radar reflectivity) or a type of integral quantity (e.g., accumulated rainfall or average flash-extent density) from the forecast model.

The Kalman gain and beta factor for the oth observation are the same as Dowell and Wicker (2009), but with the subscripts o and superscripts k added to the observation operator values H:

$$K = \frac{\frac{1}{N-1}\sum_{n=1}^{N}(x_n^f - \overline{x}^f)[H(\mathbf{x}_n^f)_o^k - \overline{H(\mathbf{x}^f)}_o^k]}{\sigma^2 + \frac{1}{N-1}\sum_{n=1}^{N}[H(\mathbf{x}_n^f)_o^k - \overline{H(\mathbf{x}^f)}_o^k]^2}, \tag{A1}$$

$$\beta = \left[1 + \sqrt{\frac{\sigma^2}{\sigma^2 + \frac{1}{N-1}\sum_{n=1}^{N}[H(\mathbf{x}_n^f)_o^k - \overline{H(\mathbf{x}^f)}_o^k]^2}}\right]^{-1}, \tag{A2}$$

where σ is the uncertainty for the observation. The superscript f indicates the state value before the assimilation of the current observation, which may have been updated already by previous observations.

The superscript k indicates that the operator value has been updated by the previous $o - 1$ observations, so $k = o - 1$, but the separate variables are used for clarity of meaning. The model state mean values $\overline{x}$ and state variables x are updated for observation o, where W is the localization factor (Gaspari and Cohn 1999). The update to the mean is given by

$$\overline{x}^a = \overline{x}^f + WK[y^o - \overline{H(\mathbf{x}^f)}_o^k] \tag{A3}$$

and the state variable analysis value is

$$\begin{aligned} x_n^a &= \overline{x}^a + (x_n^f - \overline{x}^f) + WK\beta[\overline{H(\mathbf{x}^f)}_o^k - H(\mathbf{x}_n^f)_o^k] \\ &= x_n^f + WK\{y^o - \overline{H(\mathbf{x}^f)}_o^k + \beta[\overline{H(\mathbf{x}^f)}_o^k - H(\mathbf{x}_n^f)_o^k]\}, \end{aligned} \tag{A4}$$

where the observation value is y^o. The superscript a indicates the state value after the assimilation of the current observation.

The extra step for the Anderson and Collins (2007) parallel algorithm is to update the H values corresponding to the remaining observations (for all $p > o$). The beta factor remains the same as above, and the Kalman gain K_H is simply adapted to update H instead of x:

$$K_H = \frac{\frac{1}{N-1}\sum_{n=1}^{N}[H(\mathbf{x}_n^f)_p^k - \overline{H(\mathbf{x}^f)}_p^k][H(\mathbf{x}_n^f)_o^k - \overline{H(\mathbf{x}^f)}_o^k]}{\sigma^2 + \frac{1}{N-1}\sum_{n=1}^{N}[H(\mathbf{x}_n^f)^k - \overline{H(\mathbf{x}^f)}^k]^2}. \quad \text{(A5)}$$

The mean and individual values for each observation operator are updated in the same manner as for x:

$$\overline{H(\mathbf{x}^f)}_p^{k+1} = \overline{H(\mathbf{x}^f)}_p^k + WK_H[y^o - \overline{H(\mathbf{x}^f)}_o^k], \quad \text{(A6)}$$

$$\begin{aligned} H(\mathbf{x}_n^f)_p^{k+1} &= \overline{H(\mathbf{x}^f)}_p^{k+1} + [H(\mathbf{x}_n^f)_p^k - \overline{H(\mathbf{x}^f)}_p^k] + WK_H\beta[\overline{H(\mathbf{x}^f)}_o^k - H(\mathbf{x}_n^f)_o^k] \\ &= H(\mathbf{x}_n^f)_p^k + WK_H\{y^o - \overline{H(\mathbf{x}^f)}_o^k + \beta[\overline{H(\mathbf{x}^f)}_o^k - H(\mathbf{x}_n^f)_o^k]\}. \end{aligned} \quad \text{(A7)}$$

The previous k values are not needed and, therefore in practice, are simply replaced with the new value $k + 1$.

REFERENCES

Alexander, G. D., J. A. Weinman, V. M. Karyampudi, W. S. Olson, and A. C. Lee, 1999: The effect of assimilating rain rates derived from satellites and lightning on the forecasts of the 1993 superstorm. *Mon. Wea. Rev.,* **127,** 1433–1457, doi:10.1175/1520-0493(1999)127<1433:TEOARR>2.0.CO;2.

Anderson, J. L., and N. Collins, 2007: Scalable implementations of ensemble filter algorithms for data assimilation. *J. Atmos. Oceanic Technol.,* **24,** 1452–1463, doi:10.1175/JTECH2049.1.

Betz, H. D., K. Schmidt, P. Laroche, P. Blanchet, W. P. Oettinger, E. Defer, Z. Dziewit, and J. Konarski, 2009: LINET—An international lightning detection network in Europe. *Atmos. Res.,* **91,** 564–573, doi:10.1016/j.atmosres.2008.06.012.

Brooks, I. M., C. P. R. Saunders, R. P. Mitzeva, and S. L. Peck, 1997: The effect on thunderstorm charging of the rate of rime accretion by graupel. *Atmos. Res.,* **43,** 277–295, doi:10.1016/S0169-8095(96)00043-9.

Carey, L. D., and S. A. Rutledge, 1996: A multiparameter radar case study of the microphysical and kinematic evolution of a lightning producing storm. *J. Meteor. Atmos. Phys.,* **59,** 33–64, doi:10.1007/BF01032000.

Chang, D.-E., J. A. Weinman, C. A. Morales, and W. S. Olson, 2001: The effect of spaceborne microwave and ground-based continous lightning measurements on forecasts of the 1998 Groundhog Day storm. *Mon. Wea. Rev.,* **129,** 1809–1833, doi:10.1175/1520-0493(2001)129<1809:TEOSMA>2.0.CO;2.

Christian, H. J., R. J. Blakeslee, and S. J. Goodman, 1992: Lightning imaging sensor (LIS) for the earth observing system. Tech. Rep. NASA Tech. Memo. 4350, NASA, Washington, DC, 36 pp. [Available online at http://ntrs.nasa.gov/archive/nasa/casi.ntrs.nasa.gov/19920010794.pdf.]

Cohen, A. E., 2008: Flash rate, electrical, microphysical, and kinematic relationships across a simulated storm spectrum. M.S. thesis, School of Meteorology, University of Oklahoma, Norman, OK, 71 pp.

Dowell, D. C., and L. J. Wicker, 2009: Additive noise for storm-scale ensemble data assimilation. *J. Atmos. Oceanic Technol.,* **26,** 911–927, doi:10.1175/2008JTECHA1156.1.

——, F. Zhang, L. J. Wicker, C. Snyder, and N. A. Crook, 2004: Wind and temperature retrievals in the 17 May 1981 Arcadia, Oklahoma, supercell: Ensemble Kalman filter experiments. *Mon. Wea. Rev.,* **132,** 1982–2005, doi:10.1175/1520-0493(2004)132<1982:WATRIT>2.0.CO;2.

Evensen, G., 1994: Sequential data assimilation with a nonlinear quasi-geostrophic model using Monte-Carlo methods to forecast error statistics. *J. Geophys. Res.,* **99,** 10 143–10 162, doi:10.1029/94JC00572.

Fierro, A. O., and J. M. Reisner, 2011: High-resolution simulation of the electrification and lightning of hurricane Rita during the period of rapid intensification. *J. Atmos. Sci.,* **68,** 477–494, doi:10.1175/2010JAS3659.1.

——, E. R. Mansell, C. L. Ziegler, and D. R. MacGorman, 2012: Application of a lightning data assimilation technique in the WRF-ARW Model at cloud-resolving scales for the tornado outbreak of 24 May 2011. *Mon. Wea. Rev.,* **140,** 2609–2627, doi:10.1175/MWR-D-11-00299.1.

Gaspari, G., and S. E. Cohn, 1999: Construction of correlation functions in two and three dimensions. *Quart. J. Roy. Meteor. Soc.,* **125,** 723–757, doi:10.1002/qj.49712555417.

Goodman, S. J., D. E. Buechler, P. D. Wright, and W. D. Rust, 1988: Lightning and precipitation history of a microburst-producing storm. *Geophys. Res. Lett.,* **15,** 1185–1188, doi:10.1029/GL015i011p01185.

——, and Coauthors, 2012: The GOES-R proving ground: Accelerating user readiness for the next-generation geostationary environmental satellite system. *Bull. Amer. Meteor. Soc.,* **93,** 1029–1040, doi:10.1175/BAMS-D-11-00175.1.

——, and Coauthors, 2013: The GOES-R geostationary lightning mapper (GLM). *Atmos. Res.,* **125–126,** 34–49, doi:10.1016/j.atmosres.2013.01.006.

Gurka, J. J., T. J. Schmit, T. M. Renkevens, M. M. Gunshor, and J. Li, 2006: 2006 update on baseline instruments for the GOES-R series. *Proc. SPIE,* **6301,** doi:10.1117/12.683701.

Hakim, G. J., P. Regulski, C. Mass, and R. D. Torn, 2008: Lightning data assimilation using an ensemble Kalman filter. *Extended Abstracts, 20th Int. Lightning Detection Conf.,* Tucson, AZ, Vaisala, 6 pp. [Available online at http://www.vaisala.com/en/events/ildcilmc/Documents/Lightning%20Data%20Assimilation%20using%20an%20Ensemble%20Kalman%20Filter.PDF.]

Houtekamer, P. L., and H. L. Mitchell, 1998: Data assimilation using an ensemble Kalman filter technique. *Mon. Wea. Rev.,* **126,** 796–811, doi:10.1175/1520-0493(1998)126<0796:DAUAEK>2.0.CO;2.

Kuhlman, K. M., C. L. Ziegler, E. R. Mansell, D. R. MacGorman, and J. M. Straka, 2006: Numerically simulated electrification and lightning of the 29 June 2000 STEPS supercell storm. *Mon. Wea. Rev.,* **134,** 2734–2757, doi:10.1175/MWR3217.1.

Lay, E. H., R. H. Holzworth, C. J. Rodger, J. N. Thomas, O. Pinto Jr., and R. L. Dowden, 2004: WWLL global lightning detection system: Regional validation study in Brazil. *Geophys. Res. Lett.,* **31,** L03102, doi:10.1029/2003GL018882.

MacGorman, D. R., D. W. Burgess, V. Mazur, W. D. Rust, W. L. Taylor, and B. C. Johnson, 1989: Lightning rates relative to tornadic storm evolution on 22 May 1981. *J. Atmos. Sci.,* **46,** 221–250, doi:10.1175/1520-0469(1989)046<0221:LRRTTS>2.0.CO;2.

Mach, D. M., H. J. Christian, R. J. Blakeslee, D. J. Boccippio, S. J. Goodman, and W. L. Boeck, 2007: Performance assessment of the optical transient detector and lightning imaging sensor. *J. Geophys. Res.,* **112,** D09210, doi:10.1029/2006JD007787.

Mansell, E. R., and C. L. Ziegler, 2013: Aerosol effects on simulated storm electrification and precipitation in a two-moment bulk microphysics model. *J. Atmos. Sci.,* **70,** 2032–2050, doi:10.1175/JAS-D-12-0264.1.

——, D. R. MacGorman, C. L. Ziegler, and J. M. Straka, 2002: Simulated three-dimensional branched lightning in a numerical thunderstorm model. *J. Geophys. Res.,* **107,** doi:10.1029/2000JD000244.

——, ——, ——, and ——, 2005: Charge structure and lightning sensitivity in a simulated multicell thunderstorm. *J. Geophys. Res.,* **110,** D12101, doi:10.1029/2004JD005287.

——, C. L. Ziegler, and D. R. MacGorman, 2007: A lightning data assimilation technique for mesoscale forecast models. *Mon. Wea. Rev.,* **135,** 1732–1748, doi:10.1175/MWR3387.1.

——, ——, and E. C. Bruning, 2010: Simulated electrification of a small thunderstorm with two-moment bulk microphysics. *J. Atmos. Sci.,* **67,** 171–194, doi:10.1175/2009JAS2965.1.

Meng, Z., and F. Zhang, 2007: Tests of an ensemble Kalman filter for mesoscale and regional-scale data assimilation. Part II: Imperfect model experiments. *Mon. Wea. Rev.,* **135,** 1403–1423, doi:10.1175/MWR3352.1.

Nag, A., M. J. Murphy, K. L. Cummins, A. E. Pifer, and J. A. Cramer, 2014: Recent evolution of the U.S. National Lightning Detection Network. *Extended Abstracts, 23rd International Lightning Detection Conf.,* Tucson, AZ, Vaisala, 6 pp. [Available online at http://www.vaisala.com/Vaisala%20Documents/Scientific%20papers/2014%20ILDC%20ILMC/ILDC-Wednesday/Nag%20et%20al-Recent%20Evolution%20of%20the%20U.S.%20National%20Lightning%20Detection%20Network-2014-ILDC-ILMC.pdf.]

Papadopoulos, A., T. G. Chronis, and E. N. Anagnoststou, 2005: Improving convective precipitation forecasting through assimilation of regional lightning measurements in a mesoscale model. *Mon. Wea. Rev.,* **133,** 1961–1977, doi:10.1175/MWR2957.1.

Pessi, A. T., and S. Businger, 2009: The impact of lightning data assimilation on a winter storm simulation over the North Pacific Ocean. *Mon. Wea. Rev.,* **137,** 3177–3195, doi:10.1175/2009MWR2765.1.

Petersen, W. A., H. J. Christian, and S. A. Rutledge, 2005: TRMM observations of the global relationship between ice water content and lightning. *Geophys. Res. Lett.,* **32,** L14819, doi:10.1029/2005GL023236.

Rison, W., R. J. Thomas, P. R. Krehbiel, T. Hamlin, and J. Harlin, 1999: A GPS-based three-dimensional lightning mapping system: Initial observations in central New Mexico. *Geophys. Res. Lett.,* **26,** 3573–3576, doi:10.1029/1999GL010856.

Saunders, C. P. R., and S. L. Peck, 1998: Laboratory studies of the influence of the rime accretion rate on charge transfer during crystal/graupel collisions. *J. Geophys. Res.,* **103,** 13 949–13 956, doi:10.1029/97JD02644.

Thomas, R. J., P. R. Krehbiel, W. Rison, T. Hamlin, D. J. Boccippio, S. J. Goodman, and H. J. Christian, 2000: Comparison of ground-based 3-dimensional lightning mapping observations with satellite-based LIS observations in Oklahoma. *Geophys. Res. Lett.,* **27,** 1703–1706, doi:10.1029/1999GL010845.

Weisman, M. L., and J. B. Klemp, 1982: The dependence of numerically simulated convective storms on vertical wind shear and buoyancy. *Mon. Wea. Rev.,* **110,** 504–520, doi:10.1175/1520-0493(1982)110<0504:TDONSC>2.0.CO;2.

Whitaker, J. S., and T. M. Hamill, 2002: Ensemble data assimilation without perturbed observations. *Mon. Wea. Rev.,* **130,** 1913–1924, doi:10.1175/1520-0493(2002)130<1913:EDAWPO>2.0.CO;2.

Wiens, K. C., S. A. Rutledge, and S. A. Tessendorf, 2005: The 29 June 2000 supercell observed during STEPS. Part II: Lightning and charge structure. *J. Atmos. Sci.,* **62,** 4151–4177, doi:10.1175/JAS3615.1.